Ground-state properties of the mixed-valence cobaltites $Nd_{0.7}Sr_{0.3}CoO_3$, $Nd_{0.7}Ca_{0.3}CoO_3$ and $Pr_{0.7}Ca_{0.3}CoO_3$

2013 J. Phys.: Condens. Matter 25 216006

(http://iopscience.iop.org/0953-8984/25/21/216006)

J. Phys.: Condens. Matter **25** (2013) 216006 (12pp) doi:10.1088/0953-8984/25/21/216006

Ground-state properties of the mixed-valence cobaltites $Nd_{0.7}Sr_{0.3}CoO_3$, $Nd_{0.7}Ca_{0.3}CoO_3$ and $Pr_{0.7}Ca_{0.3}CoO_3$

Z Jirák[1], J Hejtmánek[1], K Knížek[1], M Maryško[1], P Novák[1], E Šantavá[1], T Naito[2] and H Fujishiro[2]

[1] Institute of Physics ASCR, Cukrovarnická 10, 162 00 Prague 6, Czech Republic
[2] Faculty of Engineering, Iwate University, 4-3-5 Ueda, Morioka 020-8551, Japan

E-mail: jirak@fzu.cz

Received 15 January 2013, in final form 9 April 2013
Published 3 May 2013
Online at stacks.iop.org/JPhysCM/25/216006

Abstract

The electric, magnetic, and thermal properties of three perovskite cobaltites with the same 30% hole doping and ferromagnetic ground state were investigated down to very low temperatures. With decreasing size of large cations, the ferromagnetic Curie temperature and spontaneous moments of cobalt are gradually suppressed: $T_C = 130$ K, 55 K and 25 K and $m = 0.68\ \mu_B$, $0.34\ \mu_B$ and $0.23\ \mu_B$ for $Nd_{0.7}Sr_{0.3}CoO_3$, $Pr_{0.7}Ca_{0.3}CoO_3$ and $Nd_{0.7}Ca_{0.3}CoO_3$, respectively. The moment reduction with respect to the moment of the conventional ferromagnet $La_{0.7}Sr_{0.3}CoO_3$ ($T_C = 230$ K, $m = 1.71\ \mu_B$) in the so-called low spin/intermediate spin (IS/LS) state for Co^{3+}/Co^{4+} was originally interpreted using a phase-separation scenario. Based on the present results, mainly the analysis of the Schottky peak originating from Zeeman splitting of the ground-state Kramers doublet of Nd^{3+}, we find, however, that the ferromagnetic phase in $Nd_{0.7}Ca_{0.3}CoO_3$ and likely also in $Pr_{0.7}Ca_{0.3}CoO_3$ is uniformly distributed over the whole sample volume, despite the severe drop of moments. The ground state of these compounds is identified with the LS/LS-related phase derived theoretically by Sboychakov *et al* (2009 *Phys. Rev.* B **80** 024423). The ground state of $Nd_{0.7}Sr_{0.3}CoO_3$ with an intermediate cobalt moment is inhomogeneous due to competition between the LS/LS and IS/LS phases. In the theoretical part of the study, the crystal field split levels for $4f^3$ (Nd^{3+}), $4f^2$ (Pr^{3+}) and $4f^1$ (Ce^{3+} or Pr^{4+}) are calculated and their magnetic characteristics are presented.

(Some figures may appear in colour only in the online journal)

1. Introduction

In the perovskite cobaltites, two prototypical behaviors can be distinguished. The first one is associated with spin transition, or spin-state crossover of Co^{3+} ions in $LaCoO_3$ and its rare earth analogs, while the second one is manifested by a robust ferromagnetic metallic ground state that is observed in the mixed-valence $La_{1-x}Sr_xCoO_3$ systems above a critical doping value of $x = 0.22$ and exists up to the formally pure Co^{4+} end compound $SrCoO_3$ [1–3].

It is well established that the ground state of $LaCoO_3$ is based on non-magnetic low spin (LS, t_{2g}^6) states. With temperature increasing above ~40 K the energetically close HS (high spin, $t_{2g}^4e_g^2$) species start to be populated by thermal excitation. The process is readily seen in the course of magnetic susceptibility or in anomalous terms of the lattice expansion due to the ionic size of HS being notably larger than that of LS (see e.g. [4]). These experiments show that the HS population increases gradually with the steepest rate at ~80 K, and is practically saturated above 150 K, comprising about 40–50%. Strong HS/LS nearest neighbor correlations or even short-range ordering are anticipated in this phase [5–7]. At still higher temperature the ordering melts, which is accompanied by a drop of the electrical resistivity and

thermopower values at about 530 K, reminiscent of the I–M transition. The character of the high-temperature phase is not yet recognized. Intermediate spin (IS) Co^{3+} states ($t_{2g}^5 e_g^1$) have been tentatively suggested [8, 9, 7], but very recent LDA + DMFT calculations did not reveal any significant amount of IS Co^{3+} in the fluctuating mixture of spin states in $LaCoO_3$ at high temperatures [10].

The metallic conductivity in $La_{1-x}Sr_xCoO_3$ systems with stable ferromagnetic ground state is related to fast valence fluctuations that involve various $3d^N$ ($N = 5$–7) states on cobalt sites [11]. In particular, for $La_{0.7}Sr_{0.3}CoO_3$, the dominant population is the IS/LS states for Co^{3+}/Co^{4+}, so that the electronic structure can be approximated as $t_{2g}^5\sigma^{*0.7}$, where σ^* is an antibonding band of the e_g parentage. This yields a spontaneous moment of 1.70 μ_B, in agreement with 1.71(2) μ_B determined by neutron diffraction (Curie temperature $T_C = 230$ K) [1, 2]. The spontaneous moment increases with further hole doping, but most of the published data for $x > 0.5$ are influenced by severe oxygen deficiency of the samples. Nevertheless, the nearly pure Co^{4+} system $SrCoO_3$ has been prepared under very high pressures, yielding a moment of 2.5 μ_B ($T_C = 305$ K) [3]. This means that electrons are not depopulated from the e_g-derived σ^* band but from the more localized t_{2g} levels, so that, in gross simplification, the final electronic structure of $SrCoO_3$ can be presented as $t_{2g}^4\sigma^{*1}$ (see [11] for a more detailed description).

As far as the transition range between $LaCoO_3$ and $La_{0.7}Sr_{0.3}CoO_3$ is concerned, significant data have been obtained in the single crystal studies of He *et al* [12, 13]. The $La_{1-x}Sr_xCoO_3$ systems above $x = 0.22$ show characteristics of conventional ferromagnets. The ferromagnetic–paramagnetic (FM–PM) transition is manifested by a large λ peak in the specific heat and by the presence of a sharp critical scattering peak in small-angle neutron scattering at T_C. As shown in recent re-investigation of the critical exponents β, γ and δ by Khan *et al*, the transition is unambiguously of second order, characterized by scaling behavior that belongs to the universality class of the 3D Heisenberg model [14]. In contrast, in single crystal samples below $x = 0.22$ the anomalies at T_C are absent or smeared out, pointing to a much more complex temperature behavior including magnetic/electronic phase separation. The magnetic inhomogeneity of low-doped $La_{1-x}Sr_xCoO_3$ has also been proved in inelastic neutron diffraction by Phelan *et al* [15] or in NMR study by Smith *et al* [16].

The two regimes of behavior in $La_{1-x}Sr_xCoO_3$, separated by the critical doping $x = 0.22$, have been interpreted theoretically by Sboychakov *et al* [17]. Based on a fermionic model of Hubbard type, two possible FM ground states that may coexist on a nanoscopic scale are found. One is derived from the phase characterized by an LS/LS state for Co^{3+}/Co^{4+}, in which only a few Co^{3+} t_{2g} electrons are promoted to itinerant e_g levels with increasing strontium doping. The second phase is an IS/LS state for Co^{3+}/Co^{4+}, i.e. the already mentioned $t_{2g}^5\sigma^*$ phase, which becomes dominant above the critical composition $x_c \sim 0.20$. The model phase diagram presented in [17] thus reproduces remarkably well the features actually observed in the $La_{1-x}Sr_xCoO_3$ system.

The properties of mixed-valence cobaltites can be further modified by control of the ionic size on perovskite A sites. Many studies have been carried out on the $Pr_{1-x}Ca_xCoO_3$ system that exists in a limited range up to $x \sim 0.55$ [18, 19]. The substitution of smaller Pr^{3+} and Ca^{2+} ions for La^{3+} and Sr^{2+} ions causes larger size misfit between the A and B sites of the perovskite structure (Goldschmidt's tolerance factor is reduced), which results in larger deviation of the Co–O–Co bond angles from the ideal 180° and, subsequently, in narrowing of the e_g-derived band. The reduced bandwidth is detrimental not only for macroscopic conductivity but also for ferromagnetic interactions mediated by itinerant e_g electrons (the double exchange). Ferromagnetism is thus suppressed and, at the same time, the LS Co^{3+} states are promoted due to the larger t_{2g}–e_g gap. As an ultimate effect we may mention the peculiar behavior of $Pr_{1-x}Ca_xCoO_3$ systems within the range $x = 0.50$–0.55; these exhibit a sharp first-order transition to a low-temperature highly resistive and weakly magnetic state. It is of interest that the transition is associated with a charge transfer between the cobalt and praseodymium sites, resulting in a stabilization of formally Pr^{4+} states; see e.g. [20, 21] and references therein. In the region of 30% electron hole doping, on which our study is focused, pronounced effects of competing ground states were reported for $Pr_{0.7}Ca_{0.3}CoO_3$, as well as for $Nd_{0.7}Ca_{0.3}CoO_3$, and the phase-separated nature of these compounds was guessed also from the magnetization values, which are severely reduced compared to $La_{0.7}Sr_{0.3}CoO_3$ ones [22–25].

More direct information on the temperature dependence of magnetic/electronic phase separation was recently provided by the neutron diffraction, small-angle scattering, and magnetometry study of $Pr_{0.7}Ca_{0.3}CoO_3$ by El-Khatib *et al* [25]. The study showed that FM clusters (presumably hole-rich objects) were formed at a well-defined temperature $T^* \sim 250$ K, while the hole-poor PM matrix was transformed to long-range FM order at a much lower temperature $T_C = 70$ K. It is of interest that the preformed clusters did not dissolve immediately, but were preserved well below 70 K. This unusual coexistence of short- and long-range ordered FM phases possessing different coercivities was further supported by observation of exchange-spring behavior, which is known for artificial hard–soft magnetic composites [25]. It should be noted that such a behavior refers to a temperature range of 50–70 K only. The aim of this study is to resolve the final magnetic composition in $Pr_{0.7}Ca_{0.3}CoO_3$ and related compounds at the lowest temperatures.

Our paper reports on an electric, magnetic, and heat capacity investigation of selected 30% doped systems, in decreasing order of tolerance factors $Nd_{0.7}Sr_{0.3}CoO_3$, $Pr_{0.7}Ca_{0.3}CoO_3$ and $Nd_{0.7}Ca_{0.3}CoO_3$. The respective spontaneous moments are determined as 0.68 μ_B, 0.34 μ_B and 0.23 μ_B ($T_C = 130, 55$ and 25 K). Such a drop of magnetization compared to 1.71 μ_B in $La_{0.7}Sr_{0.3}CoO_3$ possessing a robust IS/LS phase was previously interpreted within the phase-separation scenario, supposing that FM ordered regions of higher hole doping are embedded in the non-magnetic matrix of low hole doping [22–25]. The present results contradict this conjecture. Based on detailed

characterization and novel application of Kramers ions Nd^{3+} as a local probe of the magnetic ground state, we show that the internal field formed by cobalt spins is uniformly distributed over the sample volume. The presence of gross magnetic/electronic phase separation in $Nd_{0.7}Ca_{0.3}CoO_3$ or $Pr_{0.7}Ca_{0.3}CoO_3$ at the lowest temperatures is thus questioned. We argue that the ground state of these samples is in fact the FM saturated LS/LS-derived phase suggested by Sboychakov *et al* [17].

2. Experimental details

Polycrystalline samples of $Nd_{0.7}Sr_{0.3}CoO_3$, $Pr_{0.7}Ca_{0.3}CoO_3$ and $Nd_{0.7}Ca_{0.3}CoO_3$ were prepared using a solid-state reaction. Raw powders of Pr_6O_{11}, Nd_2O_3, Y_2O_3, Co_3O_4, $CaCO_3$ and $SrCO_3$ were weighted with proper molar ratios and ground using an agate mortar and pestle for 1 h. The mixed powders were calcinated at 1000 °C for 24 h in air. They were subsequently pulverized and ground. Then they were pressed into pellets of 20 mm diameter and 4 mm thickness. The pellets were sintered at 1200 °C for 24 h in 0.1 MPa flowing oxygen gas. The measured density of each sample was greater than 90% of the ideal density. Powder x-ray diffraction patterns were taken for each sample using Cu Kα radiation; the samples were confirmed to have a single phase orthoperovskite (*Pbnm*) structure. The lattice parameters and volumes per f.u. actually obtained were $a = 5.364$ Å, $b = 5.409$ Å, $c = 7.599$ Å, $V/Z = 55.11$ Å^3 for $Nd_{0.7}Sr_{0.3}CoO_3$, $a = 5.363$ Å, $b = 5.351$ Å, $c = 7.570$ Å, $V/Z = 54.32$ Å^3 for $Pr_{0.7}Ca_{0.3}CoO_3$ and $a = 5.344$ Å, $b = 5.342$ Å, $c = 7.549$ Å, $V/Z = 53.87$ Å^3 for $Nd_{0.7}Ca_{0.3}CoO_3$. The present values are in agreement with the literature data for the same compounds [22, 26]. As far as the important question of the oxygen stoichiometry is concerned, practically ideal oxygen content of 2.99 ± 0.01 was evidenced for the $Pr_{0.7}Ca_{0.3}CoO_3$ specimen by Rietveld refinement of the high resolution neutron diffraction data [27]. The same seems to be valid for other two compounds based on indirect arguments, which follow from thermopower data presented below.

The electrical resistivity and thermoelectric power were measured using a four-probe method with a parallelepiped sample cut from the sintered pellet. The electrical current density varied in dependence on the sample resistivity between 10^{-1} A cm^{-2} (metallic state) and 10^{-7} A cm^{-2} (insulating state). The measurements were made during cooling and warming of the sample. In the low-temperature range, a closed-cycle cryostat working down to 2–3 K was used. For the high-temperature experiments up to 1000 K the sample was placed on a ceramic sample holder centered in a small tubular furnace with precisely controlled temperature. Standard chromel–alumel thermocouples were used to monitor of the temperature gradient around 5 K, imposed across the sample by means of an additional small furnace.

The magnetic measurements were carried out using a SQUID magnetometer MPMS-XL (Quantum Design) in the temperature range 2–400 K. The zero-field-cooled (ZFC) and field-cooled (FC) susceptibilities were measured under different applied fields. The initial AC susceptibility ($H = 0$) was studied in the frequency region 0.12–87.4 Hz using a driving AC field of 3.9 Oe. The virgin magnetization curves and hysteresis loops (−70 kOe, 70 kOe) in the ZFC regimes were recorded for selected temperatures starting from $T = 2$ K. In addition to this, the FC hysteresis loops were measured after cooling the sample from $T = 300$ to 2 K under an applied field of 70 kOe.

The specific heat was measured by a PPMS device (Quantum Design) using the two-τ model. The data were collected during sample cooling. The experiments at very low temperatures (down to 0.4 K) were performed using the ^{3}He option.

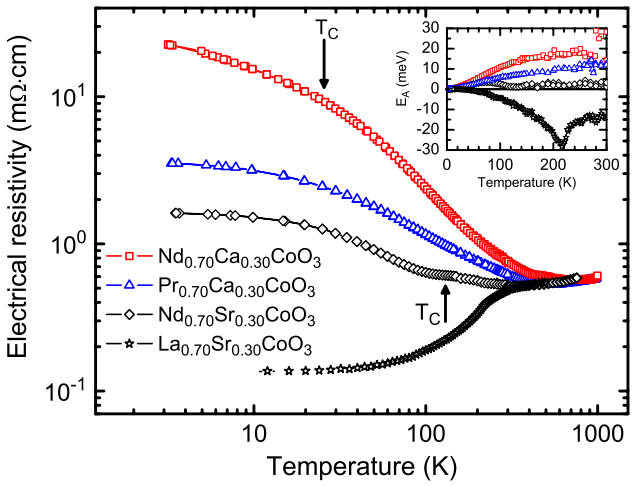

Figure 1. Resistivity of the $Nd_{0.7}Sr_{0.3}CoO_3$, $Pr_{0.7}Ca_{0.3}CoO_3$ and $Nd_{0.7}Ca_{0.3}CoO_3$ ceramic samples. Results for $La_{0.7}Sr_{0.3}CoO_3$ ceramics are added for comparison. The inset shows that, except for $Nd_{0.7}Ca_{0.3}CoO_3$, the apparent activation energy, defined as $E_A = k\mathrm{d}(\ln\rho)/\mathrm{d}(1/T)$, is below the thermal energy in the whole temperature range (the full line refers to kT).

3. Results

3.1. Electric transport

Resistivity data obtained on ceramic samples of $Nd_{0.7}Sr_{0.3}CoO_3$, $Pr_{0.7}Ca_{0.3}CoO_3$ and $Nd_{0.7}Ca_{0.3}CoO_3$ are presented in the log–log plot in figure 1. As far as the important question on metallic or insulating character of these systems is concerned, we argue that the bulk properties are generally influenced by the sample granularity, which also seems to be so in the present case. Namely, the measured resistivity steadily increases with decreasing temperature but, instead of divergence at the lowest temperatures, it extrapolates to finite values of about 1–10 mΩ cm at zero K, satisfying the criterion for metallic ground state, $\mathrm{d}(\ln\rho)/\mathrm{d}(\ln T) \to 0$ [28]. Another signature for intrinsic metallicity is the apparent activation energy, defined as $E_A = k\mathrm{d}(\ln\rho)/\mathrm{d}(1/T)$. It does not exceed the thermal energy k_BT, except for slightly enlarged E_A values for $Nd_{0.7}Ca_{0.3}CoO_3$

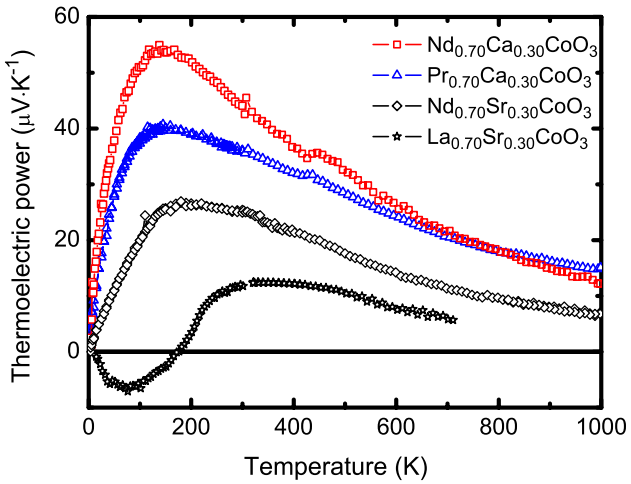

Figure 2. The thermopower data for $Nd_{0.7}Sr_{0.3}CoO_3$, $Pr_{0.7}Ca_{0.3}CoO_3$, $Nd_{0.7}Ca_{0.3}CoO_3$ and $La_{0.7}Sr_{0.3}CoO_3$.

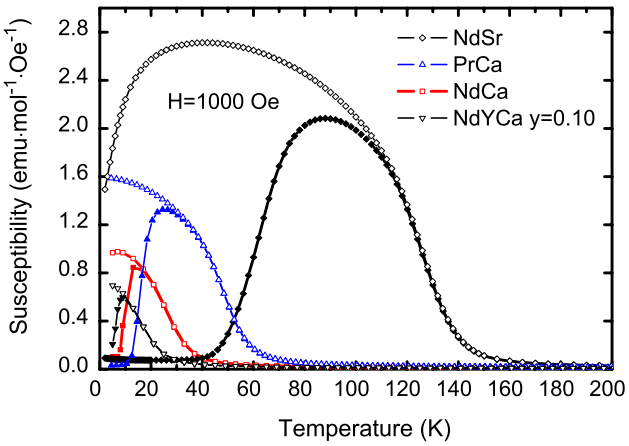

Figure 3. The zero-field-cooled (full symbols) and field-cooled (open symbols) curves of DC susceptibility in $Nd_{0.7}Sr_{0.3}CoO_3$, $Pr_{0.7}Ca_{0.3}CoO_3$ and $Nd_{0.7}Ca_{0.3}CoO_3$, measured at a field of 1000 Oe. The effect of an additional disorder is demonstrated by the data for $(Nd_{1-y}Y_y)_{0.7}Ca_{0.3}CoO_3$ ($y = 0.10$).

above T_C (see the inset of figure 1). On the other hand, the thermopower data are rather insensitive to the presence of grain boundaries. The Seebeck coefficient is positive over the whole temperature range, pointing to a hole character of the carriers (figure 2). The low-temperature dependence is of linear (metallic-like) type, but soon tends to a maximum at about 150 K, which reaches ∼25, 40 and 55 μV K^{-1} for $Nd_{0.7}Sr_{0.3}CoO_3$, $Pr_{0.7}Ca_{0.3}CoO_3$ and $Nd_{0.7}Ca_{0.3}CoO_3$, respectively. Then the thermopower slowly decreases toward a plateau of 20 μV K^{-1} at high temperatures. Let us note that the maximum values of thermopower are indirect but very sensitive indicators of the hole doping level and, based on close agreement with data on samples oxygenated under 60 atm pressure in the work of Masuda *et al* [26], they attest to an oxygen stoichiometry close to the ideal one for our compounds.

The electric properties of $Nd_{0.7}Sr_{0.3}CoO_3$, $Pr_{0.7}Ca_{0.3}CoO_3$ and $Nd_{0.7}Ca_{0.3}CoO_3$ differ substantially from the behavior of analogously prepared $La_{0.7}Sr_{0.3}CoO_3$ ceramics, for which the data have been added to figures 1 and 2. First, the resistivity in the $La_{0.7}Sr_{0.3}CoO_3$ sample shows a typical metallic dependence with a resistivity drop below $T_C \sim 220$ K. This becomes still more evident in the graph of the apparent activation energy. A more important signature of a different ground state is, however, the change of thermopower to negative values at low temperatures, in the case of $La_{0.7}Sr_{0.3}CoO_3$ pointing to a dominant role of the electron carriers of e_g parentage. On the other hand, the above mentioned hole character of the thermopower in $Nd_{0.7}Sr_{0.3}CoO_3$, $Pr_{0.7}Ca_{0.3}CoO_3$ and $Nd_{0.7}Ca_{0.3}CoO_3$ suggests that the transport of e_g carriers is impeded due to the band narrowing and/or depopulation, and the t_{2g} band becomes the prevalent conducting channel.

3.2. Magnetic properties

The magnetism in the presently studied systems is governed by the cobalt spins and their exchange interactions. The contribution of rare earths is manifested by Curie-like susceptibility with effective moments that agree very well with free-ion values at intermediate and high temperatures, $\mu_{eff} \sim 3.5\ \mu_B$ for both Nd^{3+} and Pr^{3+}. However, a significant deviation from this behavior is observed below ∼50 K, where the effects of crystal field splitting on the 4f shell become important. The low-temperature properties then depend critically on the character of the rare-earth ground state, which is a Kramers doublet for Nd^{3+} in the low-symmetry crystal field of perovskite A sites, while the non-Kramers ions Pr^{3+} possess a singlet state. This issue is discussed in detail below in section 3.3 and the appendix.

The basic magnetic characterization of $Nd_{0.7}Sr_{0.3}CoO_3$, $Pr_{0.7}Ca_{0.3}CoO_3$ and $Nd_{0.7}Ca_{0.3}CoO_3$ is represented by the ZFC and FC susceptibilities χ_{ZFC} and χ_{FC} measured in a field of 1000 Oe (figure 3). Starting from room temperature, both susceptibilities increase with decreasing temperature, and the onset of FM phase (Curie temperature) can be specified from the inflection point of the $\chi_{FC}(T)$ dependence. This yields $T_C = 130$, 55 and 25 K for $Nd_{0.7}Sr_{0.3}CoO_3$, $Pr_{0.7}Ca_{0.3}CoO_3$ and $Nd_{0.7}Ca_{0.3}CoO_3$, respectively. With further decrease of temperature, the χ_{ZFC} curves exhibit a maximum at a temperature decreasing with the increasing applied field. The χ_{FC} data for $Pr_{0.7}Ca_{0.3}CoO_3$ increase steadily toward zero temperature, while those for $Nd_{0.7}Sr_{0.3}CoO_3$ and $Nd_{0.7}Ca_{0.3}CoO_3$ show a sudden decrease at the lowest temperatures. Such a drop is caused by Nd^{3+} moments that are induced by the FM order in the cobalt subsystem and orient antiparallel to the Co^{3+}/Co^{4+} spins. See, e.g., the magnetic and neutron diffraction study of a $Nd_{1-x}Sr_xCoO_3$ sample with $x = 0.33$ by Krimmel *et al* [29]. This effect is not seen in the $Pr_{0.7}Ca_{0.3}CoO_3$ sample since the singlet ground state of Pr^{3+} lacks an intrinsic moment and shows only weak magnetic polarization that arises due to mixing with excited states.

The inverse susceptibility data are presented in a broader range of temperature in figure 4. The curvature above T_C, which is marked for $Nd_{0.7}Ca_{0.3}CoO_3$ and $Pr_{0.7}Ca_{0.3}CoO_3$ but

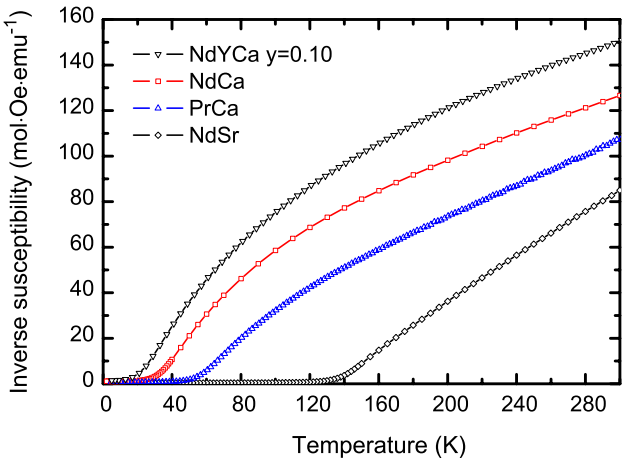

Figure 4. The inverse susceptibility for $Nd_{0.7}Sr_{0.3}CoO_3$, $Pr_{0.7}Ca_{0.3}CoO_3$, $Nd_{0.7}Ca_{0.3}CoO_3$ and $(Nd_{1-y}Y_y)_{0.7}Ca_{0.3}CoO_3$ ($y = 0.10$), based on FC data.

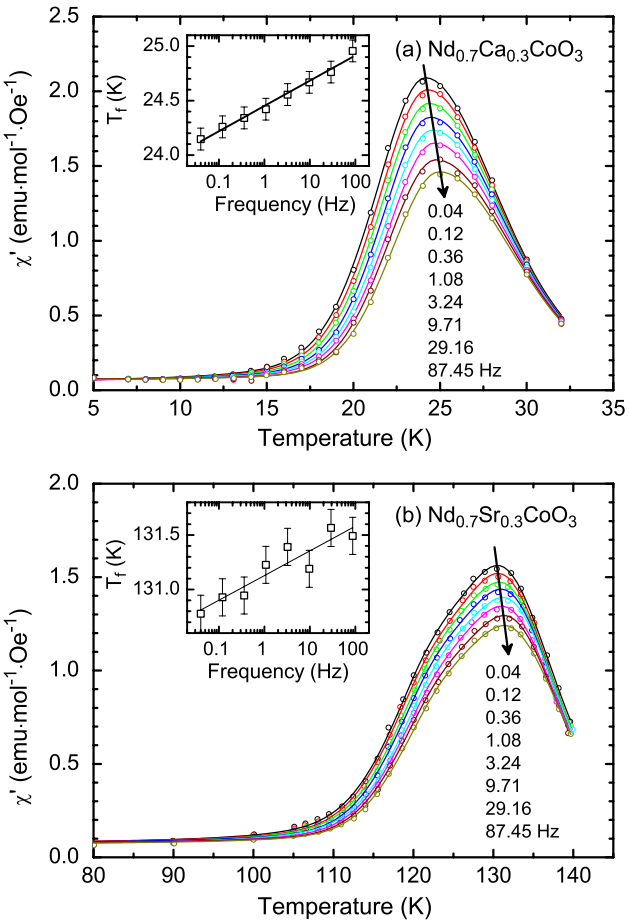

Figure 5. The real part of the AC susceptibility for $Nd_{0.7}Ca_{0.3}CoO_3$ and $Nd_{0.7}Sr_{0.3}CoO_3$. The experimental data are marked by the symbols; the full lines represent the least-squares fit of the peak form. The inset shows the frequency dependence of the freezing temperature T_f, corresponding to the susceptibility maximum.

hardly visible for $Nd_{0.7}Sr_{0.3}CoO_3$, represents a characteristic behavior for samples with ferrimagnetic ground state. This suggests that not only the Co–Nd but also the Co–Pr exchange are of antiferromagnetic (AFM) kind.

Taking into account the complexity of exchange interactions and crystal field effects, no definite conclusions on the cobalt spin states and their temperature dependence can be drawn from the low-temperature susceptibility data. A simpler situation occurs close to room temperature, where the inverse susceptibility approaches a linear Curie–Weiss behavior. The slope for $Nd_{0.7}Sr_{0.3}CoO_3$ gives, after subtraction of the free-ion value for the Nd^{3+} contribution, an effective moment of $\mu^2_{\rm eff} \sim 10\ \mu^2_{\rm B}$ per Co. This is exactly the theoretical value for an IS/IS Co^{3+}/Co^{4+} mixture, which corroborates the results for $La_{1-x}Sr_xCoO_3$ in the 300–600 K range reported by Wu and Leighton [2]. On the other hand, the asymptotic behavior of the high-temperature inverse susceptibility data for $Pr_{0.7}Ca_{0.3}CoO_3$ and $Nd_{0.7}Ca_{0.3}CoO_3$ gives notably larger effective moments of $\mu^2_{\rm eff} \sim 15$ and $19\ \mu^2_{\rm B}$ per Co, respectively, which may suggest that the Co^{3+} occur partially in the HS state as is the case for $LaCoO_3$ at room temperature. This conjecture seems to be supported by the observed Weiss temperature θ that changes from positive (FM, case of $Nd_{0.7}Sr_{0.3}CoO_3$) to negative (AFM, case of $Pr_{0.7}Ca_{0.3}CoO_3$ and $Nd_{0.7}Ca_{0.3}CoO_3$) values. With larger disorder, the AFM interactions strengthen, as clearly seen for the $Nd_{0.7}Ca_{0.3}CoO_3$ sample with yttrium doping, added to figures 3 and 4. Although the AFM interactions between cobalt and rare earths may play some role, we relate such drastic change of the magnetic interactions at high temperature mainly to the presence of excited HS Co^{3+} states in the matrix of dominant LS or IS Co^{3+} character.

The behavior of $Nd_{0.7}Ca_{0.3}CoO_3$ and $Nd_{0.7}Sr_{0.3}CoO_3$ in the vicinity of the FM transition has been further probed by AC susceptibility, for which the real and imaginary parts both culminate near T_C. For $Nd_{0.7}Ca_{0.3}CoO_3$ it is clearly seen that the characteristic temperature T_f, at which the real part χ' passes through a maximum, exhibits an upward shift with increasing frequency ν of the applied AC field (figure 5). In analogy to freezing processes in spin-glass systems, this shift can be quantified by a semiempirical dimensionless parameter $K = \Delta T_f/[T_f \Delta(\log \nu)]$. The value of this parameter was evaluated from the linear approximation of the dependence $T_f(\log \nu)$ (see the inset of figure 5) using the least-squares method, which yields $K = 0.0095 \pm 0.0005$. For $Nd_{0.7}Sr_{0.3}CoO_3$, where the frequency shift is less obvious, the analysis gives $K = 0.0017 \pm 0.0003$. The existence of a finite frequency shift means that some glassiness or 'glassy ferromagnetism' is involved in a broad range below T_C, and this refers not only to weakly magnetic $Nd_{0.7}Ca_{0.3}CoO_3$ but also to $Nd_{0.7}Sr_{0.3}CoO_3$ with a stronger FM ground state.

The virgin magnetization curves and ZFC hysteresis loops in fields up to 70 kOe are presented in figure 6. The results at the lowest temperatures show a superposition of a nearly rectangular hysteresis loop with a linear component that is mostly due to the rare-earth contribution. As expected for the magnetic ground state of Kramers ions Nd^{3+}, this additional term (paraprocess) is especially large for $Nd_{0.7}Sr_{0.3}CoO_3$ and $Nd_{0.7}Ca_{0.3}CoO_3$, while it is much smaller and apparently temperature independent for $Pr_{0.7}Ca_{0.3}CoO_3$. The spontaneous magnetization values for

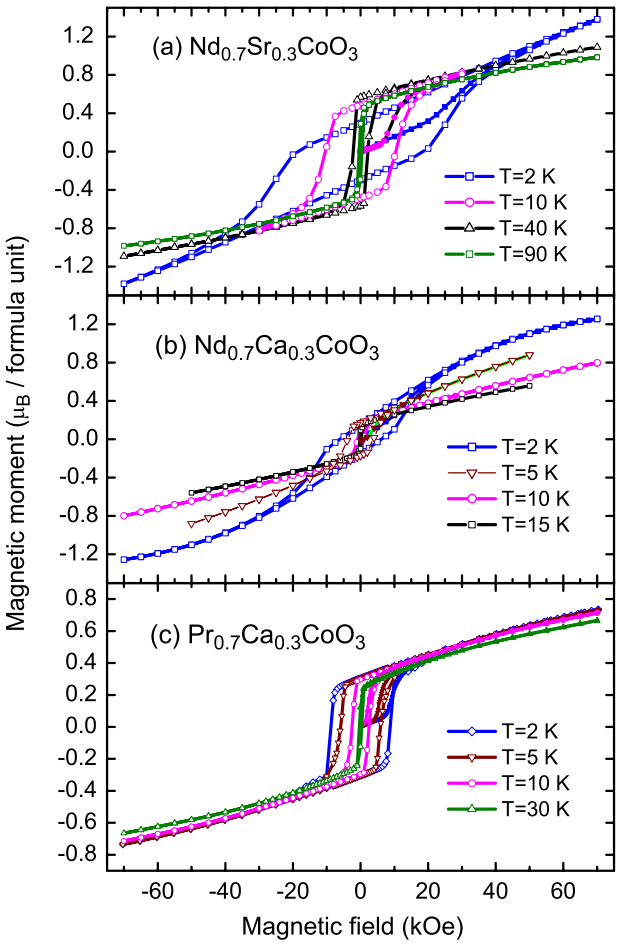

Figure 6. The virgin magnetization curves and ZFC hysteresis loops for $Nd_{0.7}Sr_{0.3}CoO_3$ (a), $Nd_{0.7}Ca_{0.3}CoO_3$ (b) and $Pr_{0.7}Ca_{0.3}CoO_3$ (c), taken at selected temperatures between T_C and 2 K.

the Co subsystem, estimated by linear extrapolation to zero field, are 0.68, 0.34 and 0.23 μ_B/Co for $Nd_{0.7}Sr_{0.3}CoO_3$, $Pr_{0.7}Ca_{0.3}CoO_3$ and $Nd_{0.7}Ca_{0.3}CoO_3$, respectively. (In order to eliminate the contribution of Nd^{3+} moments in antiparallel alignment, the extrapolation was made using hysteresis curves at higher temperatures, 40 K for $Nd_{0.7}Sr_{0.3}CoO_3$ and 10 K for $Nd_{0.7}Ca_{0.3}CoO_3$, and a small temperature correction of about 5% was applied, based rather arbitrarily on the $S = 2$ Brillouin function.) Concerning the rare-earth contribution, we note that the magnetization curve for $Nd_{0.7}Ca_{0.3}CoO_3$ at 2 K tends in high fields to a saturation of about 1.3 μ_B/f.u., which should be interpreted as a sum of μ(Co) + 0.7μ(Nd). Since our Brillouin analysis of magnetization curves in a broader temperature range did not reveal any observable paraprocess of the Co subsystem in the $Nd_{0.7}Ca_{0.3}CoO_3$ sample, we may conclude that the contribution of neodymium moments is about 1.0 μ_B, or equivalently 1.4 μ_B per Nd^{3+} ion.

The same Nd^{3+} moment can be anticipated also for the $Nd_{0.7}Sr_{0.3}CoO_3$ sample. Here, much higher fields are needed to approach magnetic saturation, because of the stronger AFM coupling between the Co and Nd subsystems. Based on a trial measurement at 2 K up to 140 kOe, we have estimated a saturated moment of 2.3 μ_B/f.u.. This may

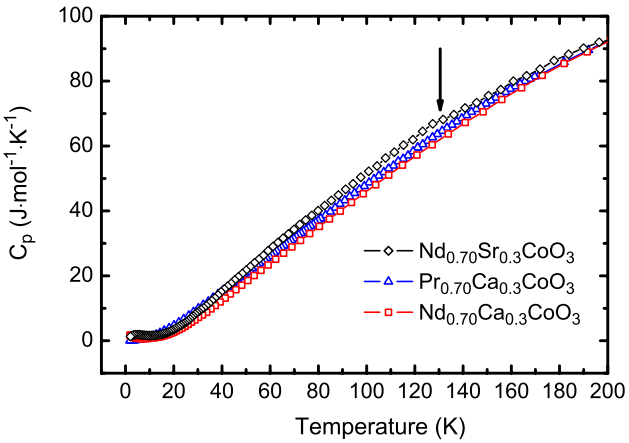

Figure 7. The heat capacity of $Nd_{0.7}Sr_{0.3}CoO_3$, $Pr_{0.7}Ca_{0.3}CoO_3$ and $Nd_{0.7}Ca_{0.3}CoO_3$ at intermediate temperatures. The arrow marks a weak anomaly at T_C for $Nd_{0.7}Sr_{0.3}CoO_3$.

signify that, unlike in $Nd_{0.7}Ca_{0.3}CoO_3$, the cobalt moment in $Nd_{0.7}Sr_{0.3}CoO_3$ increases notably under application of an external field, namely from 0.67 μ_B/Co at zero field to about 1.3 μ_B/Co at 140 kOe. The different behavior and inhomogeneous character of the $Nd_{0.7}Sr_{0.3}CoO_3$ sample has also been manifested in a shift of the center of the FC hysteresis loop toward negative fields (the exchange bias is actually 230 Oe at $T = 2$ K—not shown in figure 6(a)).

3.3. The low-temperature specific heat

The specific heat data for all studied samples are presented in a broad temperature range in figure 7. The main contribution comes from lattice dynamics, characterized by the Debye temperature $\theta_D \sim 350$–400 K for $Nd_{0.7}Sr_{0.3}CoO_3$, $Pr_{0.7}Ca_{0.3}CoO_3$ and $Nd_{0.7}Ca_{0.3}CoO_3$. In addition, there are two contributions that may affect the specific heat values at intermediate temperatures. One is the magnetic term due to cobalt ions, which is manifested by a very weak λ like anomaly at T_C in $Nd_{0.7}Sr_{0.3}CoO_3$, but is supposedly spread over a larger temperature range in $Pr_{0.7}Ca_{0.3}CoO_3$ and $Nd_{0.7}Ca_{0.3}CoO_3$. The second contribution is due to thermal excitation among the rare-earth 4f electronic levels. In the $Pr_{0.7}Ca_{0.3}CoO_3$ system with perovskite structure of the orthorhombic *Pbnm* symmetry, the $^3H_4$ electronic multiplet of Pr^{3+} is split by crystal field effects to nine singlet levels that are displaced over a large energy range of 100 meV [30]. The thermal population of the first excitation level at about 5 meV is manifested in the specific heat as a broad Schottky-type contribution, the onset of which is readily seen as a hump in the $Pr_{0.7}Ca_{0.3}CoO_3$ data at about 20 K. A more interesting situation is encountered in $Nd_{0.7}Sr_{0.3}CoO_3$ and $Nd_{0.7}Ca_{0.3}CoO_3$, where the $^4I_{9/2}$ multiplet of Nd^{3+} is split to five Kramers doublet levels [31]. Firstly, the energy gap between the ground doublet and the first excited doublet is larger, 12 meV, so that the relevant Schottky-type contribution is shifted to higher temperatures and becomes more diffusive. Secondly, the presence of an internal field due to FM ordering in the cobalt subsystem is responsible for lifting of the

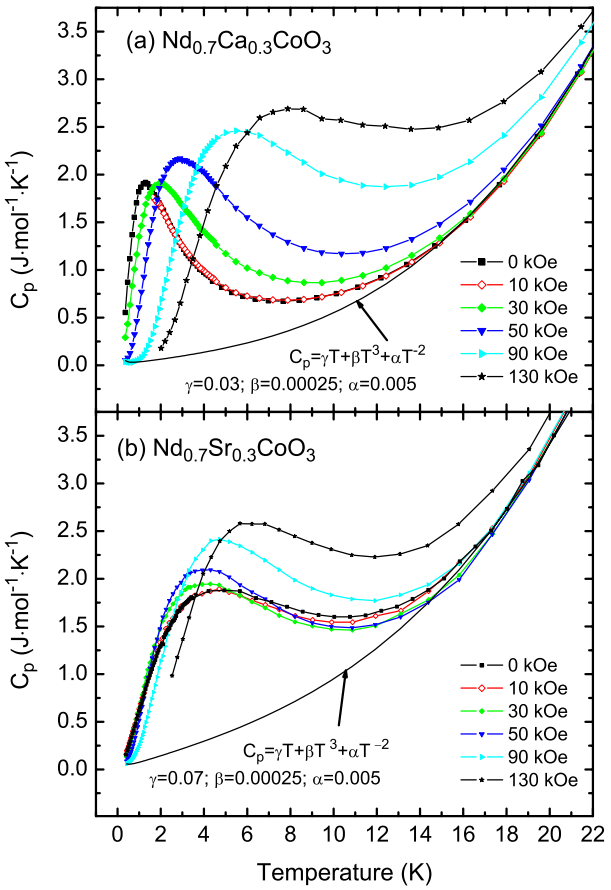

Figure 8. The low-temperature heat capacity of $Nd_{0.7}Ca_{0.3}CoO_3$ and $Nd_{0.7}Sr_{0.3}CoO_3$. The background line corresponding to a contribution of the hyperfine, lattice and linear terms is estimated with a relative uncertainty of about 5%, which reflects some ambiguity in the α, β and γ parameters.

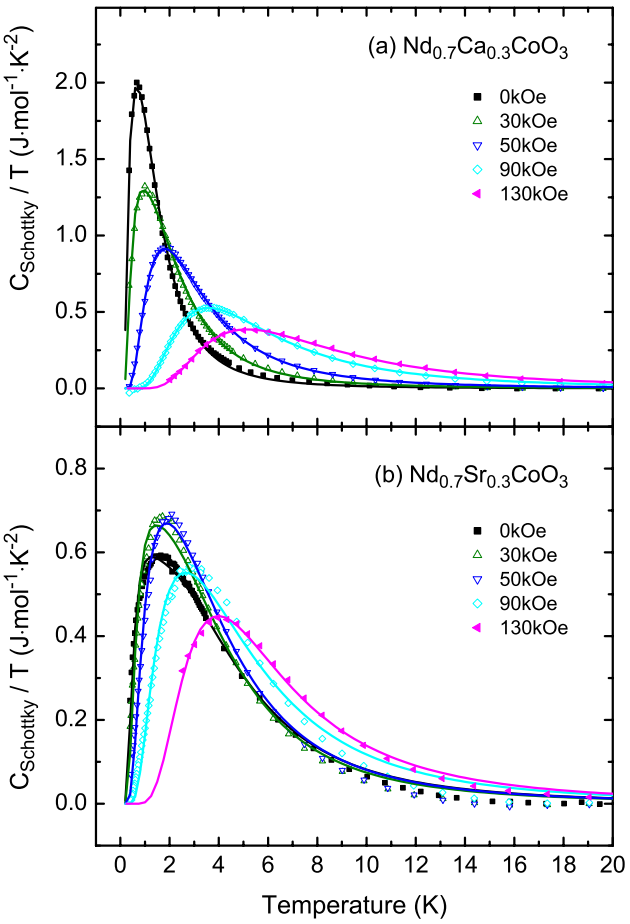

Figure 9. The heat capacity divided by the temperature for $Nd_{0.7}Ca_{0.3}CoO_3$ and $Nd_{0.7}Sr_{0.3}CoO_3$, after subtraction of the lattice and nuclear terms. The full lines present the theoretical fit based on the broadening due to anisotropic Zeeman splitting.

Kramers degeneracy of Nd^{3+} electronic states by Zeeman effects. In particular, a ground level split by an internal field is a realization of the standard two-level system for pseudospins $J' = \pm 1/2$ relevant to two eigenstates of the ground doublet. Their thermal redistribution is reflected by the appearance of a characteristic Schottky peak in the low-temperature specific heat, see e.g. [32, 33]. For the present samples, these Schottky peaks and their shift with applied magnetic field are seen in more detail in figure 8. In the subKelvin range there is another field-dependent Schottky anomaly of nuclear (^{141}Pr, $^{143/145}$Nd, ^{59}Co) origin. This T^{-2} term is especially strong for $Pr_{0.7}Ca_{0.3}CoO_3$ (not shown) because of the large Van Vleck susceptibility of praseodymium in the ground singlet state and the strong hyperfine coupling constant.

The profile of the Nd^{3+} related Schottky peaks and the location on the temperature scale ~1–10 K are controlled by Zeeman splitting of the ground doublet $-\Delta E = g_{J'}\mu_B H_{\text{eff}}$, where H_{eff} is the vector sum of internal and external fields experienced by pseudospins $J' = \pm 1/2$ in the solid-state material. The relevant data, i.e. after subtraction of the hyperfine, lattice and linear terms, are displayed as c_{Schottky}/T versus T in figure 9. Although the observed curves are broadened with respect to the ideal Schottky peak as exemplified in figure 10, no dual distribution of effective fields is found. Macroscopic phase segregation is thus ruled out. Moreover, the observed broadening does not necessarily mean inhomogeneous distribution of effective fields as it can be completely ascribed to anisotropy of the $g_{J'}$-factor and averaging in polycrystalline samples. The analysis has actually been made supposing an axial symmetry of the g-tensor for the Nd^{3+} ground doublet, so that it is described by two components $g_\parallel$ and $g_\perp$ only. This model leads to a modified Schottky form, where the energy splitting ΔE for a particular site is given by the angle θ corresponding to the deviation of the local $g_{J'}$-factor axis from the direction of the magnetic field. The partial contribution to the overall Schottky-like anomaly is calculated as $[(\Delta E_\parallel \cos\theta)^2 + (\Delta E_\perp \sin\theta)^2]^{1/2}$, and the contribution to specific heat is weighted by $\sin\theta$, which corresponds to the random orientation of crystallites in the sample. The fit, represented by solid lines in figures 9 and 10, gives for $Nd_{0.7}Ca_{0.3}CoO_3$ the ratio $\Delta E_\parallel/\Delta E_\perp = g_\parallel/g_\perp \sim 3.0$, irrespective of the strength of the applied field. The $Nd_{0.7}Sr_{0.3}CoO_3$ sample shows at $H_{\text{ext}} = 0$ and 10 kOe an excessive broadening and lower height of the Schottky peaks. At higher fields, the curves acquire a similar form and the fit gives a ratio $\Delta E_\parallel/\Delta E_\perp = g_\parallel/g_\perp \sim 4.5$. For the absolute

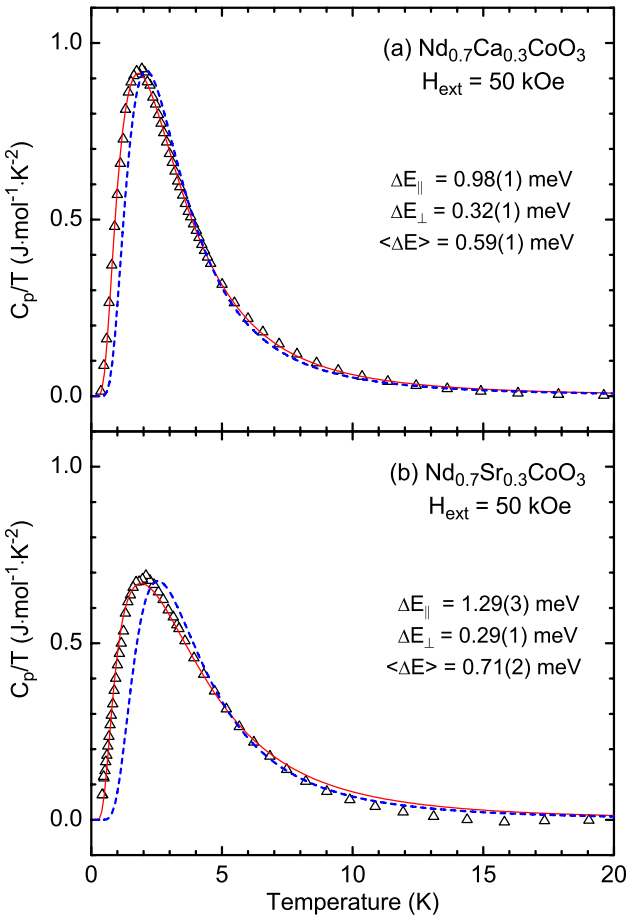

Figure 10. The c_{Schottky} contribution to the low-temperature heat capacity of $Nd_{0.7}Ca_{0.3}CoO_3$ and $Nd_{0.7}Sr_{0.3}CoO_3$ at $H_{\mathrm{ext}} = 50$ kOe. The experimental peaks and their fitted profiles in the model of anisotropic ΔE are compared with the theoretical form for an ideal Schottky peak (dashed line), which would correspond to an isotropic model with the same entropy change and splitting $\langle \Delta E \rangle$.

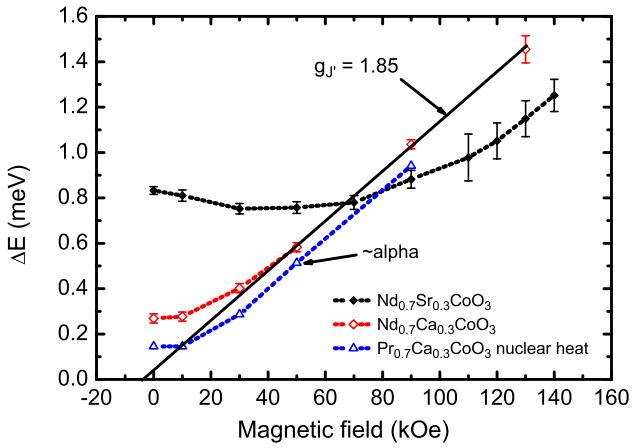

Figure 11. Average Zeeman splitting of the Nd^{3+} ground doublet for $Nd_{0.7}Ca_{0.3}CoO_3$ and $Nd_{0.7}Sr_{0.3}CoO_3$. The linear behavior for $Nd_{0.7}Ca_{0.3}CoO_3$ above $H_{\mathrm{ext}} = 50$ kOe gives $\langle g_{J'} \rangle = 1.85$. Similar dependence is observed also for the nuclear term αT^{-2} in $Pr_{0.7}Ca_{0.3}CoO_3$. The parameter α, which is proportional to the hyperfine field induced by the Van Vleck susceptibility of the Pr^{3+} electronic singlet, reaches the values 0.0034 J K mol^{-1} and 0.0220 J K mol^{-1} for $H_{\mathrm{ext}} = 0$ and 90 kOe, respectively.

values of the Zeeman splitting and g-factors, the relevant data are plotted in figure 11. It is seen that the average values of ΔE increase with external field in a gradual rate, and only at higher fields is a linear dependence approached. Since the cobalt moments are practically saturated in the Schottky peak range, the final slope seems to be a sole effect of the applied field and can thus be used to determine the $g_{J'}$-factor. The average value actually obtained for $Nd_{0.7}Ca_{0.3}CoO_3$ is $\langle g_{J'} \rangle = 1.85$. A similar field dependence is observed also in the plot of the nuclear contribution αT^{-2} for $Pr_{0.7}Ca_{0.3}CoO_3$, which probes the Van Vleck polarization of the Pr^{3+} ground singlet.

Turning back to the zero field values of $\Delta E = g_{J'}\mu_{\mathrm{B}}H_{\mathrm{eff}}$ for $Nd_{0.7}Ca_{0.3}CoO_3$ and $Nd_{0.7}Sr_{0.3}CoO_3$ (see figure 11), the spontaneous internal fields acting on the pseudospins can be determined, using the value $\langle g_{J'} \rangle = 1.85$, to be ~25 kOe and 80 kOe, respectively. The last quantity reported here is the entropy change over the Schottky peak, calculated by integration of c_{Schottky}/T. A value of 3.95 ± 0.08 J mol^{-1} K^{-1} is obtained for $Nd_{0.7}Ca_{0.3}CoO_3$, which is 98% of the theoretical value of $0.7Nk_{\mathrm{B}} \ln 2 = 4.04$ J mol^{-1} K^{-1}. For $Nd_{0.7}Sr_{0.3}CoO_3$, the value obtained from zero field data is 3.45 ± 0.07 J mol^{-1} K^{-1} and increases with increasing applied field to 3.65 ± 0.07 J mol^{-1} K^{-1}. These values correspond to 85% and 90% of the theoretical value, respectively. The increase with applied field indicates an increasing number of Nd^{3+} pseudospins contributing to the Schottky peak. The reduced entropy value at zero field, the large width of the Schottky peak showing a gradual narrowing with the applied field, and the magnetic characteristics mentioned above (paraprocess of the Co subsystem, finite exchange bias) are signatures of an inhomogeneous FM state in $Nd_{0.7}Sr_{0.3}CoO_3$.

4. Discussion

Our structural and electric transport data indicate that the $Nd_{0.7}Sr_{0.3}CoO_3$, $Pr_{0.7}Ca_{0.3}CoO_3$ and $Nd_{0.7}Ca_{0.3}CoO_3$ samples are single phase highly homogeneous polycrystalline systems of the perovskite *Pbnm* structure with oxygen stoichiometry close to the ideal one. As far as the magnetic characteristics are concerned, a comparison with available literature data on the same cobaltites is worthwhile. Both the saturated magnetic moment 0.67 μ_{B}/Co and $T_{\mathrm{C}} =$ 130 K found for the $Nd_{0.7}Sr_{0.3}CoO_3$ sample are definitely lower compared to 1.55 μ_{B}/Co and 200 K, data which were reported for a chemically most similar $Nd_{1-x}Sr_xCoO_3$ sample, nonetheless with declared slightly higher Sr content $x = 0.33$ [29]. Noting that this latter moment value is close to 1.71 μ_{B} achieved for $La_{0.7}Sr_{0.3}CoO_3$, we presume that the $Nd_{1-x}Sr_xCoO_3$ samples with $x \sim 0.3$ are close to the compositional transition from the LS/LS ground state to the IS/LS one. This can explain the large difference in magnetic response between these two samples, despite their very similar chemical compositions. Considering the two above mentioned possible ground states, the low critical temperature $T_{\mathrm{C}} = 25$ K found for our $Nd_{0.7}Ca_{0.3}CoO_3$ sample can be understood as a fingerprint of a single phase sample with LS/LS FM ground state, while a spin-glass freezing anomaly at a much

higher temperature of about 55 K reported for single crystal samples of same composition by Kundu *et al* can reflect the admixture of the IS/LS ground state with significantly higher T_C [23]. Simultaneously, we rule out a drop of the critical temperature due to oxygen deficiency in our sample (see e.g. [22]), since in spite of lower T_C we observe a 'stronger' FM state with a spontaneous moment of 0.23 μ_B/Co and significant coercivity of ~10 kOe at 2 K.

More extensive data are available for the $Pr_{0.7}Ca_{0.3}CoO_3$ system. Our sample, for which oxygen stoichiometry has been proved directly by neutron diffraction, exhibits an FM transition at $T_C = 55$ K and the spontaneous moment reaches 0.34 μ_B/Co. Identical values and similar hysteresis loops were also reported for $Pr_{0.7}Ca_{0.3}CoO_3$ by Tsubouchi *et al* [19], while other literature data cluster around higher $T_C = 70$ K and the magnitude of the bulk FM moment is generally lower. A moment of 0.15 μ_B/Co for $Pr_{0.7}Ca_{0.3}CoO_3$ is reported in the above mentioned work of Kundu *et al*. The values found on $Pr_{0.7}Ca_{0.3}CoO_3$ by El-Khatib *et al* are 0.20 μ_B as deduced from magnetization measurements and a long-range ordered moment of 0.30 μ_B/f.u. determined by neutron diffraction (this latter value is not explicitly mentioned in the paper, but can be deduced from the graph of magnetic intensities). Cobalt moments of analogous value, ~0.20 μ_B, are also obtained by Kalinov *et al* [24] on $Pr_{0.7}Ca_{0.3}CoO_3$-related systems with small A-site substitution by Eu^{3+} ions. Importantly, the magnetization curves have been measured up to high fields of 140 kOe, and the data evidence, after subtraction of the Pr contribution, a saturation of cobalt magnetization of ~0.35 μ_B/f.u.. This value is close to a sole contribution of Co^{4+} ions and evidences thus a dominance of LS/LS phase in $Pr_{0.7}Ca_{0.3}CoO_3$ systems and consequently also $Nd_{0.7}Ca_{0.3}CoO_3$.

The most significant results of the present study refer to the heat capacity experiments, namely the study and interpretation of the low-temperature Schottky peak associated with the Nd^{3+} ground-state doublet. Using this approach we have demonstrated that the presence of rare-earth ions with Kramers degeneracy can be used as a local magnetic probe in mixed-valence cobaltites. Beyond the quantitative information on entropy and level splitting, it is also possible to analyze the intrinsic or inhomogeneous broadening of the corresponding low-temperature Schottky peaks. For this purpose we have performed theoretical calculations based on the parameters of the crystal field, which have been recently deduced from extensive study of terbium aluminate, $TbAlO_3$, possessing the same *Pbnm* perovskite structure [34]. This procedure, described in detail in the appendix, provides not only the necessary characteristic energies of the energy level splitting but also the actual form of the respective doublet or singlet states. In addition to the $4f^3$ electronic configuration of Nd^{3+} and $4f^2$ for Pr^{3+}, calculations are made also for the $4f^1$ electronic configuration, which is relevant for the cases of Ce^{3+} and Pr^{4+}. Turning back to the $^4I_{9/2}$ multiplet of Nd^{3+}, the ground doublet is characterized by a highly anisotropic g-tensor with principal components $g_x = 4.472$, $g_y = 1.185$ and $g_z = 0.928$ or, in pseudoaxial approximation, $g_\parallel/g_\perp \sim 4.2$ (see table A.3 in the appendix). To enable a comparison with our experiments, a numerical integration over a random orientation of the crystallites has been made, yielding an average value of $\langle g_{J'} \rangle = 2.51$. This corresponds to a pseudospin moment of 1.255 μ_B, which is in reasonable agreement with the above mentioned saturated magnetization in $Nd_{0.7}Ca_{0.3}CoO_3$, giving an estimate of 1.4 μ_B per Nd^{3+} ion. On the other hand, the value $\langle g_{J'} \rangle = 1.85$ deduced from the high-field shift of the Schottky peaks is much lower. An opposite discrepancy has been observed for another Kramers ion Pr^{4+} in the low-temperature phase of $(Pr_{1-y}Y_y)_{0.7}Ca_{0.3}CoO_3$ with $y = 0.15$, where the shift of the Schottky peaks gives an unexpectedly large $\langle g_{J'} \rangle = 3.30$ [33], while the calculations in table A.2 in the appendix give $\langle g_{J'} \rangle = 2.07$, and a still lower value would be obtained if a correction for large Pr^{4+} covalency were made. These findings may suggest that apart from the bare interaction of the external field with the 4f moments, there is an indirect interaction through a spin polarizable electronic cloud. The same mechanism probably also mediates the exchange interaction between the FM ordered cobalt subsystem and the Kramers pseudospins for rare earths, which is of AFM type for Nd^{3+} and FM type for Pr^{4+}.[3]

5. Summary

The studied mixed-valence cobaltites are systems with complex behavior. These compounds possess an intrinsic inhomogeneity that relates to chemical and size disorder at the perovskite A sites, the possibility of various spin states at the cobalt sites, and macroscopic distortion associated with cooperative tilt of the CoO_6 octahedra. With increasing octahedral tilt (decreasing Goldschmidt tolerance factor) the FM interactions are suppressed. In particular, for $La_{0.7}Sr_{0.3}CoO_3$, $Nd_{0.7}Sr_{0.3}CoO_3$, $Pr_{0.7}Ca_{0.3}CoO_3$, and $Nd_{0.7}Ca_{0.3}CoO_3$ with the same 30% doping level, the magnetic Curie temperature gradually decreases, $T_C = 230, 130, 55$ and 25 K, and the spontaneous FM moment on cobalt sites drops, 1.71, 0.68, 0.34 and 0.23 μ_B. There is also a difference in the critical behavior around the magnetic transitions. The $La_{0.7}Sr_{0.3}CoO_3$ system behaves as a conventional ferromagnet. The systems with reduced magnetization show frequency-dependent AC susceptibility peaks, pointing to a presence of larger FM clusters for $Nd_{0.7}Sr_{0.3}CoO_3$ and smaller clusters for $Nd_{0.7}Ca_{0.3}CoO_3$ and $Pr_{0.7}Ca_{0.3}CoO_3$ in a certain temperature range below T_C. (More direct evidence of unusual behavior in the latter systems comes from small-angle neutron scattering on $Pr_{0.7}Ca_{0.3}CoO_3$, which shows a presence of preformed FM entities of 10 Å size, which only well below T_C grow to macroscopic size [25].)

The magnetization data on $Nd_{0.7}Sr_{0.3}CoO_3$, $Pr_{0.7}Ca_{0.3}CoO_3$, and $Nd_{0.7}Ca_{0.3}CoO_3$ at low temperatures exhibit standard FM hysteresis loops combined with

[3] The exchange interaction couples the cobalt spins with the spin component of the rare earth moments, which is oppositely oriented to the total momentum in the $J = L - S$ multiplet. The antiparallel orientation is valid also for projection of spin momentum in the Kramers pseudospin J'.

a paraprocess caused by rare-earth paramagnetism. The long-range character of magnetic ordering is reported also in a few neutron diffraction experiments; these, however, cannot decide whether the severely suppressed moment in $Pr_{0.7}Ca_{0.3}CoO_3$ and $Nd_{0.7}Ca_{0.3}CoO_3$ is a manifestation of a uniform phase of weakly magnetic character or refers to two phase coexistence of macroscopic FM and non-magnetic regions[4]. Using low-temperature heat capacity experiments as an efficient tool for analysis of internal magnetic fields, we decide in favor of an essentially homogeneous phase in the calcium based compounds down to nanoscopic or even atomic scale. Firstly, we note that the magnitude of the cobalt moments is remarkably close to 0.3 μ_B, which is exactly the theoretical value for a mixture of non-magnetic $S = 0$ ions of LS Co^{3+} and $S = 1/2$ ions of LS Co^{4+}. No metamagnetic increase of cobalt magnetization has been detected on application of fields up to 140 kOe. This strongly supports our conclusion that the ground state is the LS/LS phase with only minor promotion of t_{2g} electrons to itinerant e_g levels. This promotion is necessarily associated with a rise of cobalt moments, but the increased magnetization might be compensated by the presence of oppositely oriented impurity moments due to isolated $S = 2$ ions of HS Co^{3+}. Secondly, the form and intensity of the Schottky peaks originating in Zeeman splitting of the ground-state Kramers doublet of Nd^{3+} show unambiguously that all rare-earth sites experience the same effective field. The uniform distribution of hole carriers (formally LS Co^{4+}) in the main LS/LS phase is thus firmly established for $Nd_{0.7}Ca_{0.3}CoO_3$ and can be anticipated for $Pr_{0.7}Ca_{0.3}CoO_3$ as well, in order to account for the similarly reduced magnetization of the Co subsystem, ~0.3 μ_B. For the remaining compound $Nd_{0.7}Sr_{0.3}CoO_3$, the observed magnetization is intermediate between those for LS/LS in $Nd_{0.7}Ca_{0.3}CoO_3$ and IS/LS in $La_{0.7}Sr_{0.3}CoO_3$. Based on a reduced intensity of the Nd^{3+}-related Schottky peak, we infer that some rare-earth sites are located in magnetically disordered regions or, to account for the exchange bias in $Nd_{0.7}Sr_{0.3}CoO_3$, in AFM ordered regions. Such a finding is direct evidence of the inhomogeneous state of this sample.

As a final remark, let us note that the present results are closely related to the general problem of the 3d–4f exchange in perovskite oxides, mediated presumably by spin polarization of extended orbitals of rare-earth 5d parentage—see the Campbell's indirect exchange mechanism treated in [35] and references therein. It is not yet clear how the mixed-valence character of cobaltites, i.e. the presence of itinerant carriers, affects the strength and eventually also the sign of the exchange interaction. To elucidate all these issues, magnetic and heat capacity studies on twin-free single crystals are desirable. Single crystal experiments may also give a better test of the homogeneity of FM phases, probed by analysis of the actual form of the Schottky peaks, since excessive broadening due to anisotropic g-factors will be eliminated.

[4] In the theoretical case of FM–non-FM phase coexistence, the average value of the ordered moment deduced from neutron diffraction is higher than the average value deduced from magnetization data (this follows from the fact that the magnetic diffraction intensities give a root-square-mean value of the moments). This situation seems to occur for the $Pr_{0.7}Ca_{0.3}CoO_3$ sample probed by El-Khatib *et al*, but the value of 0.3 μ_B (compared to 0.2 μ_B obtained by the magnetization method) is close to the resolution limit of neutron diffraction and is thus subject to large uncertainty.

Acknowledgment

This work was supported by Project No. 204/11/0713 of the Grant Agency of the Czech Republic.

Appendix. Electron states and magnetism of lanthanide ions in orthorhombic perovskites

To describe the 4f states of lanthanide ions, a Hamiltonian that consists of the free-ion (atomic) and crystal field terms is routinely used,

$$\hat{H} = \hat{H}_a + \hat{H}_{CF}. \tag{A.1}$$

The free-ion Hamiltonian is spherically symmetrical and in a standard notation (see, for example, [36]) it can be written as

$$\begin{aligned}\hat{H}_a = E_{avg} &+ \sum_{k=2,4,6} F^k \hat{f}_k + \zeta_{4f} \sum_{i=1}^{N} \hat{s}_i \hat{l}_i + \alpha \hat{L}^2 \\ &+ \beta \hat{G}(G_2) + \gamma \hat{G}(R_2) + \sum_{j=0,2,4} M^j \hat{m}_j \\ &+ \sum_{k=2,4,6} P^k \hat{p}_k + \sum_{r=2,3,4,6,7,8} T^r \hat{t}(r),\end{aligned} \tag{A.2}$$

where E_{avg} is the energy in the central field, terms proportional to $F^k, \alpha, \beta, \gamma$ and T^r describe the electron–electron interaction, and terms with ζ_{4f}, M^j, P^k parameters represent the spin–orbit, spin–other-orbit and electrostatically correlated spin–orbit interactions. N is the number of 4f electrons.

Within single electron crystal field theory the crystal field Hamiltonian may be written as [37]

$$\hat{H}_{CF} = \sum_{k,q,i} B_q^{(k)} \hat{C}_q^{(k)}(i), \tag{A.3}$$

where $\hat{C}_q^{(k)}(i)$ is a spherical tensor operator of rank k acting on the ith electron and the summation involving i is over the f electrons of the lanthanide ion. $B_q^{(k)}$ are crystal field parameters; the values of q and k for which they are nonzero depend on the site symmetry and also on the choice of the local coordinate system. The local symmetry of the lanthanide site in orthorhombic perovskites is C_s and choosing the crystal field coordinate axes along the orthorhombic axes a, b, c results in three nonzero, real $B_0^{(k)}$ parameters ($k = 2, 4, 6$) and six nonzero complex $B_q^{(k)}$ parameters ($k = 2, 4, 6$; $q = 2, 4, 6$; $q \leqq k$). Rotation of the crystal field coordinate system around the c axis allows elimination of the imaginary part of the $B_2^{(2)}$ parameter (for detailed discussion of the crystal field in orthorhombic perovskites see [34]). The crystal field axes x, y, z, ($z \parallel c$) obtained in this way are used, in what follows, also as the reference system for lanthanide susceptibility and g tensor. Low symmetry of the crystal field leads to a complete lift of the orbital degeneracy of the 4f levels, so that the states are either singlets (N even) or Kramers doublets (N odd).

Table A.1. States of the ground $^3H_4$ multiplet of the Pr^{3+} ion split by the crystal field. The energy, relative to the ground state, at zero external magnetic field, and the magnetic moments m_x, m_y, m_z, induced by a field of 10 kOe.

State	E (meV)	m_x (μ_B)	m_y (μ_B)	m_z (μ_B)
1	0.00	0.0469	0.0308	0.0139
2	8.29	0.2765	0.0536	−0.0021
3	9.94	−0.2484	−0.0182	0.0514
4	11.57	−0.0667	−0.0302	−0.0431
5	27.57	0.0620	0.0321	0.0144
6	29.98	−0.0624	−0.0407	−0.0038
7	52.92	0.0073	0.0041	−0.0216
8	63.61	−0.0052	−0.0250	0.0743
9	74.20	−0.0081	−0.0043	−0.0811

For the free lanthanide ions the total angular momenta L, S, and J are good quantum numbers. The ground states are in accord with the Hund's rules and for Ce^{3+} (f^1), Pr^{3+} (f^2), and Nd^{3+} (f^3) they are $^2F_{5/2}$ ($S = 1/2, L = 3, J = 5/2$), $^3H_4$ ($S = 1, L = 5, J = 4$), and $^4I_{9/2}$ ($S = 3/2, L = 6, J = 9/2$), respectively. For a given lanthanide ion the values of the parameters of the atomic Hamiltonian (A.2) depend to some extent on the host compound. This dependence has little significance for the results given below, however. The crystal field is thus decisive for the low-temperature behavior of the lanthanide ions.

In order to calculate the electron states of trivalent lanthanides in orthorhombic perovskites we used the program 'lanthanide' [38], which makes it possible to determine energy levels and eigenfunctions of Hamiltonian (A.1) with an external magnetic field added. For the atomic parameters, values given by Carnall *et al* [36] were adopted. The crystal parameters $B_q^{(k)}$ were taken to be the same as those determined recently by Gruber *et al* [34] for the non-Kramers Tb^{3+} ion in terbium aluminate. The eigenenergies and magnetic moments we calculated for the $4f^8$ electron configuration practically coincide with those obtained by Gruber *et al* [34]. In particular, the energy difference between the lowest two Tb^{3+} singlets is only 0.026 meV; the very large magnetic moment (8.8 μ_B at a magnetic field of 50 kOe) has an Ising-like character with the Ising axis parallel to the x axis of the crystal field. There are two crystallographically equivalent sites of Tb^{3+} ions in the unit cell related by reflection in the ac plane. The x axis for these two sites makes an angle of $\pm 36°$ with the orthorhombic axis a.

Compared to Tb^{3+}, the Pr^{3+} ion is less anisotropic. The energies and magnetic moments of the states originating from the lowest $^3H_4$ multiplet of Pr^{3+} are given in table A.1. The dependence of the magnetic moments on the magnetic field is to a good approximation linear; only for the first and second excited states and the field parallel to the x axis is there a tendency to saturation in high magnetic fields. The induced magnetic moments are small with the exception of the first and second excited states that may be classified as an Ising-like pseudodoublet. The susceptibility χ is anisotropic and its temperature dependence is displayed in figure A.1.

Ce^{3+} and Nd^{3+} are Kramers ions with $4f^1$ and $4f^3$ electron configurations respectively. The magnetic moments

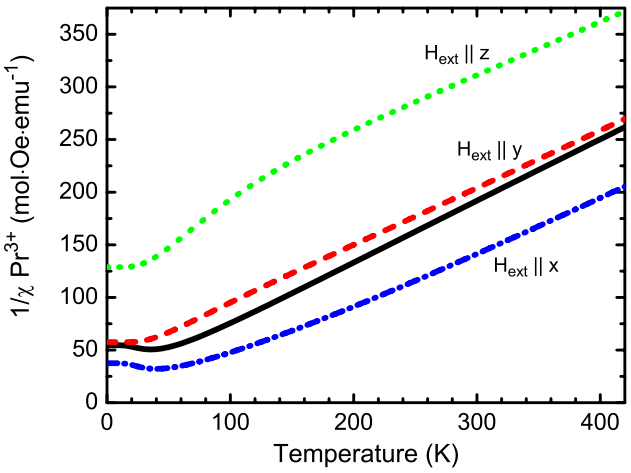

Figure A.1. The theoretical dependence of the inverse susceptibility of the Pr^{3+} ion, based on the singlet state energies in table A.1 and the calculated shifts in a field of 10 kOe. The full line corresponds to the average over random orientations; the linear Curie behavior at higher temperatures gives an effective moment of $\mu_{eff} = 3.68\ \mu_B$, in agreement with the experimental value of $\sim 3.5\ \mu_B$.

Table A.2. Three Kramers doublets of the ground $^2F_{5/2}$ multiplet of the Ce^{3+} ion split by the crystal field. The energy, relative to the ground state, at zero external magnetic field, and the g factors.

State	E (meV)	g_x	g_y	g_z
1	0.00	3.757	0.935	0.606
2	33.46	1.298	2.298	1.458
3	56.36	0.945	1.212	3.451

Table A.3. Five Kramers doublets of the ground $^4I_{9/2}$ multiplet of the Nd^{3+} ion split by the crystal field. The energy, relative to the ground state, at zero external magnetic field, and the g factors.

State	E (meV)	g_x	g_y	g_z
1	0.00	4.472	1.185	0.928
2	11.83	0.942	3.925	1.077
3	22.87	2.034	1.257	3.540
4	53.52	2.978	3.063	1.052
5	65.33	1.788	1.435	4.204

of all Kramers doublets are almost field independent: they increase by 1–5% when the field changes between 10 and 100 kOe. There is considerable anisotropy of the moment, the x axis being the easy axis of the ground doublet for both Ce^{3+} and Nd^{3+}. The g factors of the Kramers doublets may be determined by multiplying the magnetic moments by a factor of two, corresponding to a pseudospin of 1/2. The calculated energies and the g factors are summarized in tables A.2 and A.3.

References

[1] Caciuffo R, Rinaldi D, Barucca G, Mira J, Rivas J, Señarís-Rodríguez M A, Radaelli P G, Fiorani D and Goodenough J B 1999 *Phys. Rev.* B **59** 1068
[2] Wu J and Leighton C 2003 *Phys. Rev.* B **67** 174408

[3] Long Y W, Kaneko Y, Ishiwata S, Taguchi Y and Tokura Y 2011 *J. Phys.: Condens. Matter* **23** 245601
[4] Knížek K, Jirák Z, Hejtmánek J and Novák P 2006 *J. Phys.: Condens. Matter* **18** 3285
[5] Goodenough J B 1958 *J. Phys. Chem. Solids* **6** 287
[6] Bari R A and Sivardiére J 1972 *Phys. Rev.* B **5** 4466
[7] Knížek K, Jirák Z, Hejtmánek J, Novák P and Ku W 2009 *Phys. Rev.* B **79** 014430
[8] Kyômen T, Asaka Y and Itoh M 2005 *Phys. Rev.* B **71** 024418
[9] Jirák Z, Hejtmánek J, Knížek K and Veverka M 2008 *Phys. Rev.* B **78** 014432
[10] Křápek V, Novák P, Kuneš J, Novoselov D, Korotin D M and Anisimov V I 2012 *Phys. Rev.* B **86** 195104
[11] Kuneš J, Křápek V, Parragh N, Sangiovanni G, Toschi A and Kozhevnikov A V 2012 *Phys. Rev. Lett.* **109** 117206
[12] He C, El-Khatib S, Wu J, Lynn J W, Zheng H, Mitchell J F and Leighton C 2009 *Europhys. Lett.* **87** 027006
[13] He C, Eisenberg S, Jan C, Zheng H, Mitchell J F and Leighton C 2009 *Phys. Rev.* B **80** 214411
[14] Khan N, Midya A, Mydeen K, Mandal P, Loidl A and Prabhakaran D 2010 *Phys. Rev.* B **82** 064422
[15] Phelan D, Louca D, Kamazawa K, Lee S H, Ancona S N, Rosenkranz S, Motome Y, Hundley M F, Mitchell J F and Moritomo Y 2006 *Phys. Rev. Lett.* **97** 235501
[16] Smith R X, Hoch M J R, Kuhns P L, Moulton W G, Reyes A P, Boebinger G S, Mitchell J and Leighton C 2008 *Phys. Rev.* B **78** 092201
[17] Sboychakov A O, Kugel K I, Rakhmanov A L and Khomskii D I 2009 *Phys. Rev.* B **80** 024423
[18] Tsubouchi S, Kyômen T, Itoh M, Ganguly P, Oguni M, Shimojo Y, Morii Y and Ishii Y 2002 *Phys. Rev.* B **66** 052418
[19] Tsubouchi S, Kyômen T, Itoh M and Oguni M 2004 *Phys. Rev.* B **69** 144406
[20] Herrero-Martin J, García-Muñoz J L, Kvashnina K, Gallo E, Subias G, Alonso J A and Barón-González A J 2012 *Phys. Rev.* B **86** 125106
[21] Fujishiro H, Naito T, Ogawa S, Yoshida N, Nitta K, Hejtmánek J, Knížek K and Jirák Z 2012 *J. Phys. Soc. Japan* **81** 064709
[22] Kundu A K, Sampathkumaran E V, Gopalakrishnan K V and Rao C N R 2004 *J. Magn. Magn. Mater.* **281** 261
[23] Kundu A K, Nordblad P and Rao C N R 2006 *J. Solid State Chem.* **179** 923
[24] Kalinov A V *et al* 2010 *Phys. Rev.* B **81** 134427
[25] El-Khatib S, Bose S, He C, Kuplic J, Laver M, Borchers J A, Huang Q, Lynn J W, Mitchell J F and Leighton C 2010 *Phys. Rev.* B **82** 100411
[26] Masuda H, Fujita T, Miyashita T, Soda M, Yasui Y, Kobayashi Y and Sato M 2003 *J. Phys. Soc. Japan* **72** 873
[27] ORNL experiment, unpublished
[28] Möbius A and Adkins C J 2000 *Physica* B **284** 1669
[29] Krimmel A, Reehuis M, Paraskevopoulos M, Hemberger J and Loidl A 2001 *Phys. Rev.* B **64** 224404
[30] Podlesnyak A, Rosenkranz S, Fauth F, Marti W, Scheel H J and Furrer A 1994 *J. Phys.: Condens. Matter* **6** 4099
[31] Podlesnyak A, Rosenkranz S, Fauth F, Marti W, Furrer A, Mirmelstein A and Scheel H J 1993 *J. Phys.: Condens. Matter* **5** 8973
[32] Gordon J E, Fisher R A, Jia Y X, Phillips N E, Reklis S F, Wright D A and Zettl A 1999 *Phys. Rev.* B **59** 127
[33] Hejtmánek J, Šantavá E, Knížek K, Maryško M, Jirák Z, Naito T, Sasaki H and Fujishiro H 2010 *Phys. Rev.* B **82** 165107
[34] Gruber J B, Nash K L, Yow R M, Sardar D K, Valiev U V, Uzokov A A and Burdick G W 2008 *J. Lumin.* **128** 1271
[35] Richter M 1998 *J. Phys. D: Appl. Phys.* **31** 1017
[36] Carnall W T, Goodman G L, Rajnak K and Rana R S 1989 *J. Chem. Phys.* **90** 3443
[37] Wybourne B G 1965 *Spectroscopic Properties of Rare Earths* (New York: Wiley)
[38] Edvardsson S and Aberg D 2001 *Comput. Phys. Comm.* **133** 396